# Study on the Comprehensive Performance and Structural Parameters of All-Terrain Vehicle Radiators

Jie MENG, Yi XU, Hui FENG, Yan WANG, and Zhenyu LEI

Abstract—To enhance the heat transfer performance of louver radiators in all-terrain vehicles (ATVs) and reduce operational noise, numerical simulations were conducted using Fluent to analyze the heat transfer and noise characteristics of the radiator with varying louver angles under different operating conditions. The results indicate that the heat transfer and noise performance of the louver radiator are lower under high-load conditions compared to low-load conditions. For the same operating conditions, a larger louver angle corresponds to reduced heat transfer performance; specifically, the JF evaluation index for a 15° louver is 66.4% higher than that for a 40° louver. The noise performance decreases as the shutter angle increases, reaching its peak at 15°, which is 42.45% higher than the lowest performance observed at 40  $^{\circ}$  . The comprehensive evaluation reveals that the optimal balance between noise and heat dissipation efficiency is achieved with a louver angle of 20  $^{\circ}\,$  , which is 25% higher than the lowest evaluation at 40°. These findings provide valuable engineering insights for the design and optimization of ATV radiators.1

Index Terms—Louvered fin radiator; Numerical simulation; Aerodynamic noise; Heat transfer factor

#### I. INTRODUCTION

ll-terrain vehicles (ATVs), known for their high mobility and adaptability, are extensively used in various fields, including military operations, rescue missions, exploration, and agriculture. Given the necessity to function effectively in challenging terrains, engine radiators are subjected to particularly rigorous demands. As a critical component of the cooling system, the radiator not only facilitates thermal management but also produces operational noise that can impact the driver's psychological well-being and health. Consequently, investigating the heat dissipation and noise performance of radiators is critically important. Radiators are available in various designs, with fins categorized by shape into types such as flat fins, corrugated fins, serrated fins, and louvered fins, as illustrated in Figure 1. This study focuses on louvered fin radiators, which are particularly effective at disrupting the fluid boundary layer.

Manuscript received June 14, 2025; revised August 20, 2025.

This study was supported by the General Program of Natural Science Research of Shanxi Province (Grant No. 202203021221148).

Jie MENG is an associate professor at the School of Vehicle and Transportation Engineering, Taiyuan University of Science and Technology, Taiyuan 030024, China (e-mail: 2018054@tyust.edu.cn).

Yi XU is a postgraduate from the School of Vehicle and Transportation Engineering, Taiyuan University of Science and Technology, Taiyuan 030024, China (e-mail: xuyi514971593@163.com).

Hui FENG is a manager at Guizhou Jonyang Kinetics Co., Ltd, Guizhou 550006, China (e-mail: fenghui@jonyang.com).

Yan WANG is a postgraduate from the School of Vehicle and Transportation Engineering, Taiyuan University of Science and Technology, Taiyuan 030024, China (e-mail: s202324211151@stu.tyust.edu.cn).

Zhenyu LEI is a manager at Guizhou Jonyang Kinetics Co., Ltd, Guizhou 550006, China (e-mail: leizhenyu@jonyang.com).

This disruption significantly enhances the heat transfer coefficient, resulting in superior heat exchange performance compared to other fin types.



(a) Flat fins.



(b) Corrugated fins.



(c) Serrated fins.



(d) Serrated fins.Fig. 1. Types of Fins.

Zeng Zhixin et al. [1] employed the SST k-ω detached eddy simulation model for their numerical analysis. Drawing inspiration from biomimetic principles based on shark dorsal fins, they designed an innovative fan blade that significantly reduces aerodynamic noise. Alessandro Zarri et al. [2] investigated the impact of low-speed fans on vehicle noise in the context of automotive engine cooling, developing a method to predict low-frequency sounds. Their approach specifically considers the influence of blade sweep angle on turbulence-induced acoustic predictions. Wojciech et al. [3] investigated the impact of orifice size on the magnitude of pressure waves in pulsating flow within straight pipes. They concluded that smaller orifice dimensions result in a reduction of pressure wave intensity. Xie Hui et al. [4] conducted experiments in a soundproof chamber to evaluate the vibration and sound pressure levels of throttle orifices with varying specifications. Their findings indicated that stepped throttle orifices demonstrate the lowest mechanical energy loss and radiated sound pressure levels. Bi Jiaming et al. [5] conducted a signal-to-noise ratio analysis on the structural variables of plate heat exchangers, identifying the chevron angle and plate height as the most significant factors influencing overall performance. Alessandro et al. [6] assessed the turbulence characteristics downstream of radiators, demonstrating that heat dissipation fins and louvers effectively mitigate vortex structures. Amoiridis et al. [7] reported that radiators equipped with thin cooling tubes and dense grids have a minimal impact on sound source localization maps and spectra. Furthermore, turbulence modeling frequently depends on isotropic and homogeneous models, such as the von Kármán or Liepmann models [8]. Hu D et al. [9] constructed a multiphysical field calculation model of the radiator based on the synergistic characteristics of the thermal-acoustic field. The magnetic field synergy angle is utilized as the evaluation index to optimize the layout of the radiator system. The results indicate that the overall heat dissipation of the optimized radiator system has increased by 8%, while the sound level of the radiator fan has been reduced by 4.2 dBA. Aiming to address the noise generated by automobile cooling systems, Park M et al. [10] investigated the acoustic characteristics of straight, front-leaning, and rear-leaning blades through numerical simulations and experiments. They predicted the noise signal at the monitoring point using the acoustic analogy method. The study concluded that the design of front-leaning blades can effectively reduce fan noise compared to rear-leaning blades. Wang S et al. [11] designed a ridged fan blade using bionic technology and investigated the effect of the ridged structure on the noise produced by the cooling fan through orthogonal experiments conducted in a semi-anechoic chamber. The results indicate that the vortices generated by the ridged structure disrupt the boundary layer flow, thereby delaying the transition of the fan blade to turbulence.

Zhang Ruijia et al. [12] investigated needle-fin radiators, focusing on the effects of various structural parameters on cooling efficiency. They conducted simulations on 16 distinct structural combinations to analyze flow and heat transfer performance, aiming to identify an optimal design. Cao Kan et al. [13] developed an innovative staggered-hole louver fin and utilized computational fluid dynamics (CFD) to simulate its performance, validating the results through

experimental data and empirical formulas. Xie Wenyuan et al. [14] incorporated jet effects into graded manifold microchannel array radiators, optimizing the cooling channel length to achieve efficient heat dissipation and reduced flow resistance. Yu Wan et al. [15] designed a micro heat pipe radiator, combining experimental methods with simulations to identify optimal operating conditions and structural configurations. Wang Di et al. [16] proposed a novel radiator fin structure and validated its effectiveness through numerical simulations, noting that triangular holes in the fins reduce flow resistance caused by triangular vortex generators. Chen Huilan et al. [17] utilized COMSOL software to simulate the heat transfer performance of perforated straight fin radiators under various optimization strategies, demonstrating that perforation designs enhance heat dissipation efficiency. Zhu Maotao et al. [18] introduced an innovative pointed cone louver fin and investigated how variations in the thickness of the middle section and louver spacing affect performance. Tang Jingchun et al. [19] conducted wind tunnel experiments to evaluate the heat transfer and resistance characteristics of radiators with different structural parameters, developing computational models for the heat transfer coefficient (j) and the friction coefficient (f) to predict performance. Yoo B.K. et al. [20] proposed an empirical relationship between the thermal coefficient and the friction coefficient of the heat exchanger, based on geometric parameters. They compared the simulation results with experimental data, and the findings indicate that both the heat transfer factor (j) and the friction factor (f) demonstrate high accuracy. Zhang X et al. [21] developed an airfoil-fin element inspired by a bionic structure. They compared and analyzed the aerodynamic characteristics of airfoil, conical, and rectangular fin configurations using three-dimensional flow simulations. The experimental data indicate that the heat transfer efficiency of the bionic fin surpasses that of traditional structures, while the flow resistance coefficient is lower, demonstrating optimal overall thermodynamic performance. Yu C [22] proposed an accurate and effective method for optimizing louvered fin heat exchangers. The optimal structural parameters were determined through computational fluid dynamics (CFD) simulations, and the structural dimensions were optimized using a multi-objective genetic algorithm.

These studies typically employ porous characteristic structures for noise analysis and use CFD simulations to compare and determine optimal parameters for louver fin dimensions. However, most research focuses exclusively on either noise or heat dissipation. Comprehensive studies addressing both the heat dissipation and noise performance of radiators remain limited.

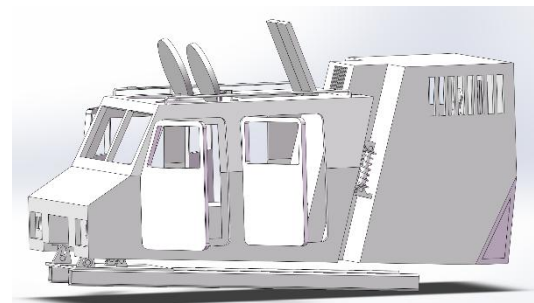
This paper uses numerical simulations to examine the effects of different louver opening angles on the heat dissipation performance and fluid noise of radiators under various operating conditions, aiming to identify optimal structural parameters that balance heat dissipation and noise reduction.

#### II. NUMERICAL MODEL OF LOUVERED FINS

#### A. Geometric Model

This study investigates louvered fin radiators, with fins constructed from aluminum alloy. Given that the engine is situated behind the driver's cabin, the radiator is positioned immediately aft of the engine, as illustrated in Figure 2(a).

To streamline the acoustic field simulation, the model was simplified by excluding the radiator's waist tube and inlet/outlet ports, as these elements have negligible effects on the acoustic and thermal characteristics being examined. The simplified overall physical model of the radiator is depicted in Figure 2(b).



(a) Schematic of the driver's cabin.



(b) Simplified radiator.

Fig. 2. Simplified radiator model.

In heat transfer simulations, leveraging the periodic arrangement and symmetry of the fins, a symmetric half of a fin within a periodic unit was modeled to represent the entire structure. The simplified louvered fin model is presented in Figure 3.

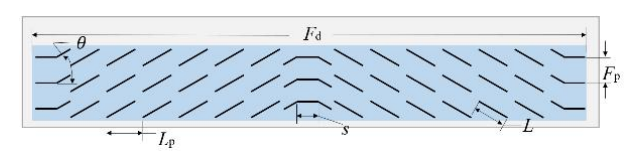


Fig. 3. Schematic of louvered fin structural parameters.

GEOMETRIC PARAMETERS OF THE LOUVERED FIN RADIATOR

Parameter	Value
Fin pitch, F <sub>p</sub> /mm	2
Louver angle, $\theta/(^{\circ})$	15/20/30/40
Fin length, L/mm	2
Louver pitch, L <sub>p</sub> /mm	2
Fin width, F <sub>d</sub> /mm	32
Transition length, S/mm	1.5

This study examines the noise and heat transfer performance of louvered fin radiators in relation to the louver angle  $\theta$ . In practical engineering applications, louver angles generally vary from  $10^{\circ}$  to  $45^{\circ}$ . Consequently, four representative angles within this range were chosen for quantitative analysis. The relevant structural parameters are detailed in Table 1.

#### B. Numerical Model

For noise simulation in this study, the Lighthill acoustic analogy method is utilized for acoustic modeling, chosen for its suitability in capturing flow-induced noise in low Mach number flows, consistent with the radiator's operational conditions. This method integrates the momentum and mass conservation equations for viscous incompressible fluids to derive the wave equation for sound propagation, including the associated sound source terms [23]. This approach is appropriate given the low Mach number flow conditions in the radiator.

The transient flow field analysis is initiated from a steady-state flow field solution. Upon reaching a stable transient state, the flow data are employed as an equivalent sound source for acoustic simulations using the Lighthill acoustic analogy method, as formulated in Equation (1):

$$\frac{\partial^{2} \rho'}{\partial t^{2}} - a_{0}^{2} \nabla^{2} \left( \frac{\partial^{2} \rho'}{\partial t^{2}} \right) - a_{0}^{2} \nabla^{2} \rho' = 
\frac{\partial}{\partial t} \left[ \rho_{0} u_{i} \frac{\partial s}{\partial x_{i}} \delta(s) \right] - \frac{\partial}{\partial x_{i}} \left[ p' \delta_{ij} \frac{\partial s}{\partial x_{i}} \delta(s) \right] + \frac{\partial^{2} T_{ij}}{\partial x_{i} \partial x_{j}}$$
(1)

where  $\rho'$  denotes the sound pressure (in Pa),  $a_0$  is the background speed of sound in the medium (in m/s),  $\nabla^2$  is the Laplacian operator, defined as the sum of second-order partial derivatives with respect to spatial coordinates, p' represents density fluctuations (in kg/m³),  $\rho_0$  is the average fluid density (in kg/m³),  $\delta_{ij}$  is the Kronecker delta, indicating the symmetry or directionality of tensor components,  $T_{ij}$  is the Lighthill stress tensor (in Pa).

For the heat transfer analysis simulation, a three-dimensional, steady-state, incompressible laminar flow model is adopted to streamline the computational analysis. This assumption is based on the low Reynolds number within the fin channels, ensuring an accurate representation of the flow regime. The continuity equation is:

$$\frac{\partial(\rho u)}{\partial x} + \frac{\partial(\rho v)}{\partial y} + \frac{\partial(\rho w)}{\partial z} = 0$$
 (2)

The momentum equation is:

$$\nabla \cdot (\rho u u_i) = -\nabla p + \nabla \cdot \tau \tag{3}$$

The energy equation is:

$$\frac{\partial}{\partial t}(\rho E) + \frac{\partial}{\partial x_i} \left[ u_i(\rho E + P) \right] =$$

$$\frac{\partial}{\partial x_i} \left( k_{\text{eff}} \frac{\partial T}{\partial x_i} - \sum_j h_j J_j + u_j (\tau_{ij})_{\text{eff}} \right) + S_h$$
(4)

Where P is the static pressure (in Pa),  $\tau_{ij}$  is the stress tensor,  $k_{\rm eff}$  is the effective thermal conductivity,  $S_h$  is the volumetric heat source term.

The heat transfer coefficient ( h ) is calculated as:

$$h_a = \frac{m_a C_{P_a} (T_W - T_i)}{A \times \Delta T_{\text{LMTD}}}$$
 (5)

The logarithmic mean temperature difference is given by:

$$T_{\text{LMTD}} = \frac{(T_i - T_w) - (T_o - T_w)}{\ln\left(\frac{T_i - T_w}{T_o - T_w}\right)}$$
(6)

Where  $m_a$  is the air mass flow rate (in kg/s),  $C_{P_a}$  is the specific heat capacity at constant pressure (in J/(kg·K)),  $T_i$ ,  $T_o$  and  $T_W$  are the air inlet temperature, air outlet temperature, and fin temperature, respectively (in K), A is the total heat transfer area of the fins (in m²).

This study employs the heat transfer factor (j), friction factor (f), and the dimensionless factor (JF), as defined by Yun and Lee [24], to evaluate the comprehensive heat transfer performance of the radiator. The JF factor combines heat transfer and friction characteristics to assess overall performance. The specific formulas for these evaluation factors are as follows:

$$j = \frac{h_a P_r^{2/3}}{\rho c_p V} \tag{7}$$

$$f = \frac{A_c}{A_a} \left( \frac{2\Delta P}{\rho V^2} - k_c - k_\varepsilon \right) \tag{8}$$

$$JF = \frac{j}{f^{1/3}} \tag{9}$$

Where  $h_a$  is the heat transfer coefficient on the fin surface (in W/(m²·K)),  $P_r$  is the Prandtl number of air,  $\rho$  is the air density (in kg/m³),  $c_p$  is the specific heat capacity of air (in J/(kg·K)), V is the air velocity (in m/s),  $A_c$  and  $A_a$  are the minimum flow area of the fluid and the total area for convective heat transfer between the fluid and solid, respectively (in m²),  $\Delta P$  is the pressure drop on the air side (in Pa),  $k_c$  and  $k_c$  are the coefficients for sudden contraction and sudden expansion pressure losses, respectively.

# C. Computational Model and Settings

During the operation of an all-terrain vehicle (ATV), the engine's rotational speed varies from 1500 to 3000 RPM, depending on conditions such as idling or uphill driving. This corresponds to airflow velocities at the radiator ranging from 7 m/s to 17 m/s. Accordingly, inlet velocities of 8 m/s, 10 m/s, 12 m/s, 14 m/s, and 16 m/s were selected for the simulations.

Fluent is utilized for fluid noise simulations of the radiator, employing a pressure-based coupled solver. The SIMPLE algorithm computes the steady-state flow field, followed by the Coupled algorithm for transient flow and acoustic field calculations. Once the transient flow field stabilizes, flow data from each time step are extracted as the sound source. The Lighthill volume source model calculates sound wave propagation, and a discrete Fourier transform converts time-domain signals into the frequency domain. A Hanning window function is applied to smooth the acoustic signals, reducing high-frequency noise interference and enhancing frequency analysis accuracy.

This study aims to investigate the noise distribution on the radiator's inlet side and assess the sound pressure level in the driver's cabin. To this end, a quarter-sphere acoustic monitoring area is constructed with the radiator at its center [26]. A quarter-sphere was chosen due to the symmetry of the radiator and the focus on noise propagation towards the driver's cabin. Monitoring points are placed every 15 degrees on a 3-meter radius spherical surface across the XOY, ZOY, and ZOX planes, as shown in Figure 4. Sound pressure data from these points characterize the noise distribution in the sound field.

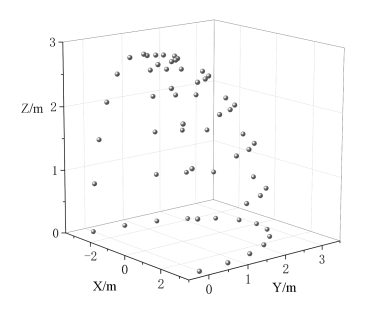


Fig. 4. Spatial monitoring point setup

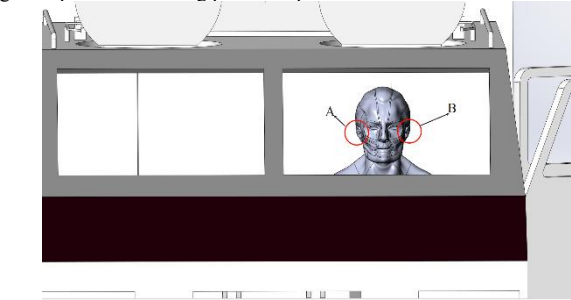


Fig. 5. Spatial monitoring point setup.

TABLE II

MONITORING FOINT LOCATIONS				
Spherical coordinates	R	Θ	Φ	
	/m	/°	/0	
A	3	45	60	
В	3	60	30	

Additionally, considering the distance between the radiator and the driver's cabin, noise monitoring points A and B are established near the driver's ear position to quantify cabin noise levels, as depicted in Figure 5. Their precise locations are specified in Table 2, where R denotes the distance from the radiator center to the monitoring point,  $\Theta$  represents the horizontal angle relative to the positive Y-axis, and  $\Phi$  indicates the elevation angle with respect to the XY plane.

In the heat transfer investigation, the same inlet velocities as those used in the noise simulation (8 m/s, 10 m/s, 12 m/s, 14 m/s, and 16 m/s) are adopted to simulate various operating conditions.

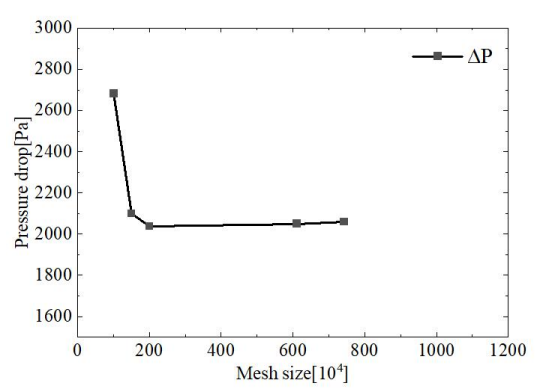
ANSYS Fluent is used to simulate the fluid heat transfer within the radiator. To mimic the actual operating conditions, the surfaces to which the fins are attached are designated as constant-temperature walls at 363 K, representing the heat source. The fins are modeled as solid regions to account for conjugate heat transfer. The inlet temperature is set to 300 K, and the outlet domain is extended to ten times the fin thickness to ensure fully developed flow and prevent backflow effects. The interface between the fluid and fins is treated as a coupled fluid-solid boundary. The Coupled algorithm is employed for velocity and pressure coupling. A laminar flow model is utilized, and the energy and momentum conservation equations are discretized using a second-order upwind scheme.

#### D. Mesh Independence Verification

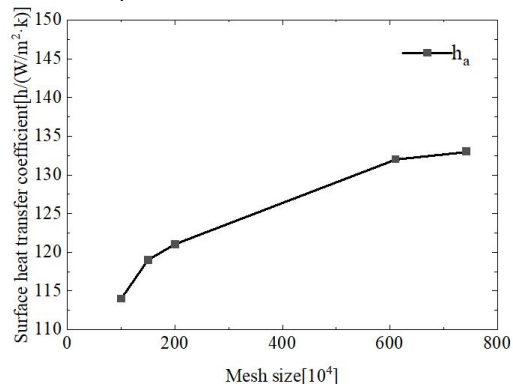
Mesh independence was verified by evaluating five different mesh sizes: 1 million, 1.5 million, 2 million, 6.1 million, and 7.43 million cells. The results, shown in Figure 6(a) and (b), indicate that a mesh with 6.1 million cells provides a suitable balance between computational accuracy and efficiency for both noise and heat transfer simulations. This mesh size was chosen as it provided converged results for both the overall sound pressure level and heat transfer

coefficient, with further refinement yielding negligible changes. The fluid domain is meshed with tetrahedral elements, while a refined Cartesian body-fitted mesh is employed at the fluid-fin interfaces, as depicted in Figure 7(a) and (b).

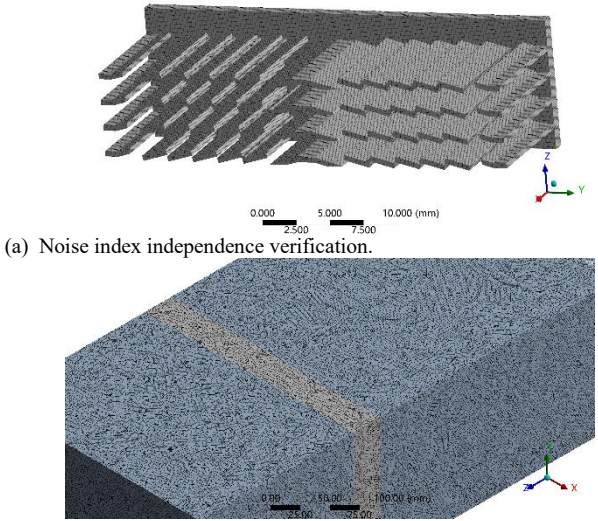
The results of the mesh independence verification are presented in Figure 6. It was observed that the pressure drop  $(\Delta P)$  stabilized as the grid count increased from 530,000 to 1,100,000, with variations remaining within 1% beyond 5,000,000 grids. To achieve a balance between computational accuracy and efficiency, a grid system consisting of 8,906,718 elements was selected for subsequent simulations.



(a) Noise index independence verification.



(b) Heat transfer index independence verification. Fig. 6. Mesh independence analysis.



(b) Etrahedral mesh for fluid domain Fig. 7. Heat dissipation fin mesh.

#### III. NOISE RESULT ANALYSIS

# A. Acoustic Field Analys

The acoustic field analysis was performed using the Lighthill acoustic analogy equation to compute sound pressure data from the source region to the monitoring points. This approach facilitates the determination of the total sound pressure level (SPL) distribution across the radiator's near-field and far-field regions, providing insights into noise characteristics relevant to radiator design. According to references [27]-[28], the sound pressure level is defined as:

$$SPL = 10 \log \left( \frac{p_{\rm ms}^2}{p_{\rm ref}^2} \right) \tag{10}$$

where SPL represents the sound pressure level (dB),  $p_{rms}$  is the fluctuating pressure (Pa), and  $p_{ref}$  is the reference sound pressure, set at 20  $\mu$ Pa.

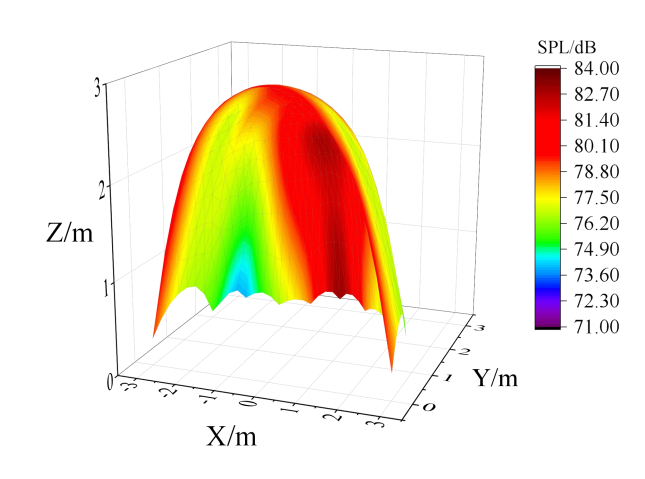
Acoustic simulation data from Fluent's monitoring sphere were processed in Origin to generate the acoustic field distribution plots. Figure 8 and Table 3 present the relative acoustic field distribution of the radiator at various louver angles, with an incoming flow velocity of v = 14 m/s.

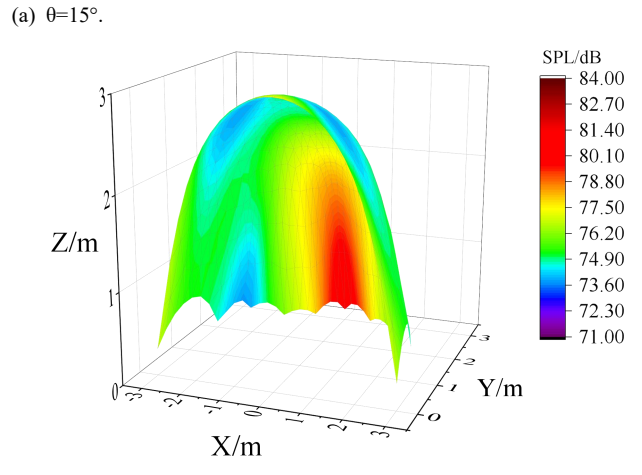
At a louver angle of 15°, the noise distribution exhibits a regular parabolic shape, with a maximum SPL of 83.88 dB, a minimum SPL of 75.62 dB, an average SPL of 78.85 dB, and an SPL range of 8.26 dB. High SPL areas are predominantly concentrated near the radiator's center, indicating that this configuration induces elevated turbulence intensity in the flow field, which increases airflow pulsating pressure and raises the peak frequency by approximately 15%.

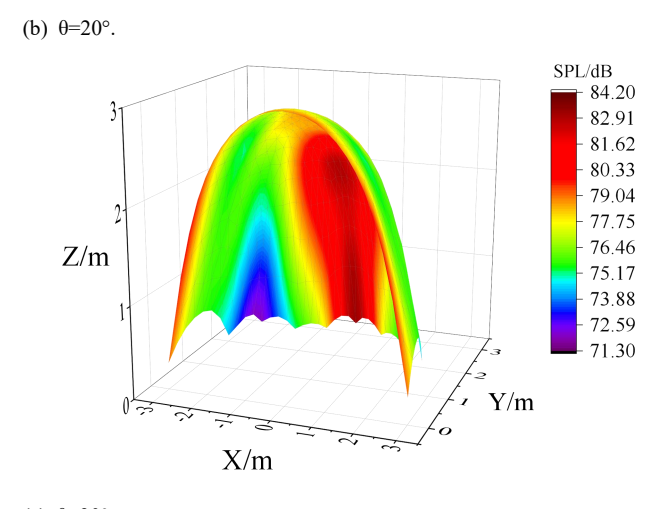
At a louver angle of 20°, as the louver angle increases, turbulence disturbances weaken, and airflow pulsating pressure decreases, leading to an overall reduction in noise levels. The maximum SPL drops to 80.84 dB (a 3.62% reduction compared to 15°), the minimum SPL decreases to 73.33 dB (a 2.29 dB reduction, or approximately 3.03%), and the average SPL falls by 3.67% to 75.96 dB. The SPL range narrows by 9.1% to 7.51 dB. Additionally, the extent of high SPL regions diminishes, and peripheral noise diffusion intensifies.

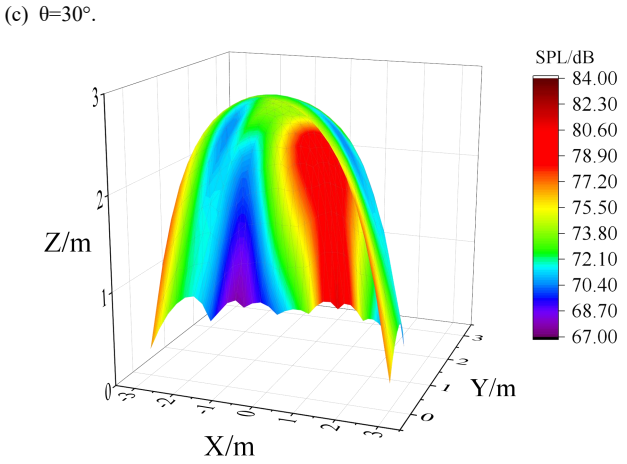
At a louver angle of 30°, further increasing the louver angle significantly reduces the uniformity of the noise distribution. The SPL range widens to 12.86 dB (a 55.7% increase compared to 15°), with the maximum SPL rising to 84.19 dB (a 4.14% increase from 20°), the highest among all configurations. The minimum SPL drops to 71.33 dB, and the average SPL increases to 77.88 dB (a rise of 1.92 dB, or approximately 2.53%). This shift suggests intensified flow separation at this angle, enhancing local turbulence intensity and resulting in a more irregular spatial distribution of sound sources.

In summary, at smaller louver angles, noise concentrates in the central region with higher overall levels. As the louver angle increases, noise levels gradually decline, peripheral diffusion strengthens, and distribution uniformity decreases.









(d)  $\theta$ =40°. Fig. 8. Acoustic field distribution at v=14 m/s.

TABLE III

OVERALL SOUND PRESSURE LEVELS.

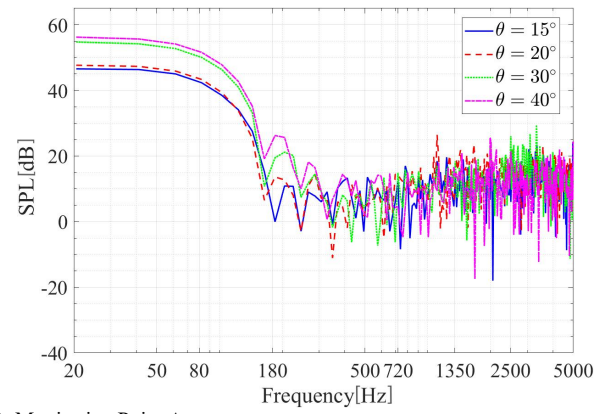
θ/°	Evaluation index	SPL/dB
	Maximum	83.88
15	Minimum	73.48
	Average	78.85
20	Maximum	80.84
	Minimum	73.33
	Average	75.96
30	Maximum	84.19
	Minimum	71.33
	Average	77.88
40	Maximum	82.31
	Minimum	67.25
	Average	73.93

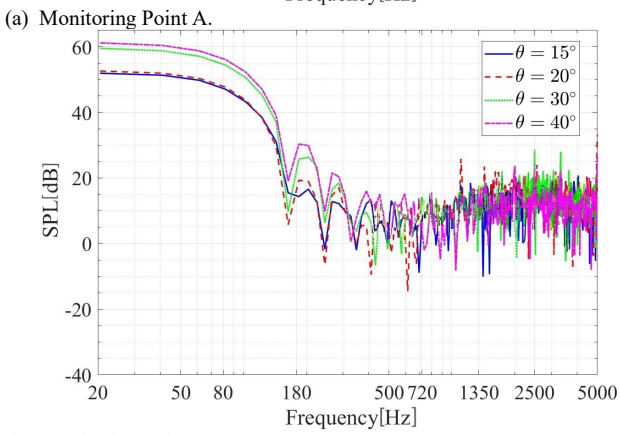
# B. Ear-Side Monitoring Point Spectrum Analysis

To further assess the louvered radiator's impact on cabin noise, sound pressure spectrum characteristics were analyzed at monitoring points A and B, located near the driver's ears within the monitoring sphere (see Table 2 for coordinates). The results, illustrated in Figures 9(a) and 9(b), highlight the following trends for both the left (A) and right (B) ear monitoring points:

In the 20–500 Hz frequency band, the SPL increases with larger louver angles.

In the 1350–5000 Hz mid-to-high frequency range, SPL fluctuations stabilize, though minor undulations remain, consistent with the broadband characteristics of turbulence noise.





(b) Monitoring Point B. Fig. 9. Sound Pressure Level Spectra at Typical Monitoring Points.

# C. Noise Evaluation Index

In order to quantify the noise performance of the radiator, this study calculated the objective parameters

related to the sound quality of the spectral data collected from monitoring points near the ear. Since loudness and sharpness effectively reflect the human ear's perception of sound intensity and harshness, these two indicators were selected as the basis for evaluating noise performance. The spectral data were analyzed according to the calculation formulas for loudness and sharpness developed by Zwicker. The results are presented in Table 4.

 $\label{total logical logical} Table\ IV$  Loudness and sharpness values at monitoring points of the radiator at different window angles

θ/°	Location of detecting	Loudness / sone	Sharpness / acum
15	Left ear	23.78	0.7525
	Right ear	24	0.7562
20	Left ear	24.96	0.7401
	Right ear	25.48	0.7559
30	Left ear	26.08	0.6037
	Right ear	26.44	0.6048
40	Left ear	23.82	0.5783
	Right ear	23.96	0.5784

It can be observed from the table that as the window opening angle increases, the loudness in both the left and right ears initially rises and then declines. In contrast, the sharpness consistently exhibits a decreasing trend with the increase in angle. Since the variations in loudness and sharpness are not entirely synchronized, this paper proposes a noise evaluation index,  $P_a$ , which is based on both loudness and sharpness to more intuitively quantify the overall characteristics of ear noise.

Firstly, the loudness and sharpness are normalized to eliminate the influence of dimensionality. The normalized loudness and sharpness are denoted as  $P_s$  and  $P_c$ , respectively, both of which are negative index parameters. A larger value indicates poorer noise performance.

According to engineering experience in the subjective evaluation of sound quality parameters for special vehicles, the weights of loudness and sharpness are determined. The expression for the noise evaluation index, P<sub>a</sub>, is as follows:

$$P_{a} = 0.71 P_{s} + 0.29 P_{c}$$
 (11)

Figure 10 illustrates the noise performance line chart for four sets of radiators, each with varying window angles, under different operating conditions (8, 10, 12, 14, and 16 m/s).

According to the analysis of the diagram, as wind speed increases, the  $P_a$  values for each window opening angle also rise, resulting in a significant enhancement of noise levels under high-speed conditions. Specifically, at a 15° window angle, the  $P_a$  of the radiator increases by 61.44% compared to the low-speed condition.

Under the same working condition of 14 m/s, the sound pressure level ( $P_a$ ) of the radiator decreases as the window opening angle increases. The maximum value occurs at an angle of 15°, indicating that the noise exhibits the poorest overall performance in terms of loudness and sharpness. In comparison, the minimum  $P_a$  at a 40° angle is approximately 42.45% lower, suggesting that a larger window opening angle significantly enhances noise performance. This trend holds true across all operating conditions, with the 40° window opening angle demonstrating the best performance. Therefore, increasing the window opening angle contributes to improved noise performance of the radiator.

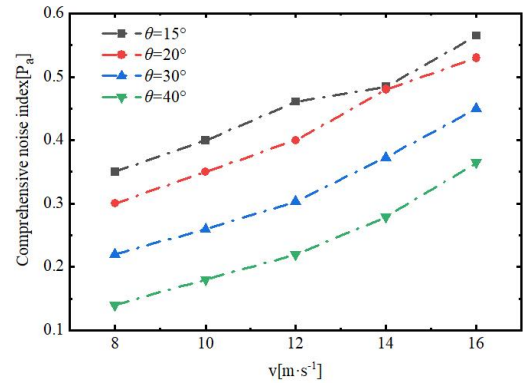
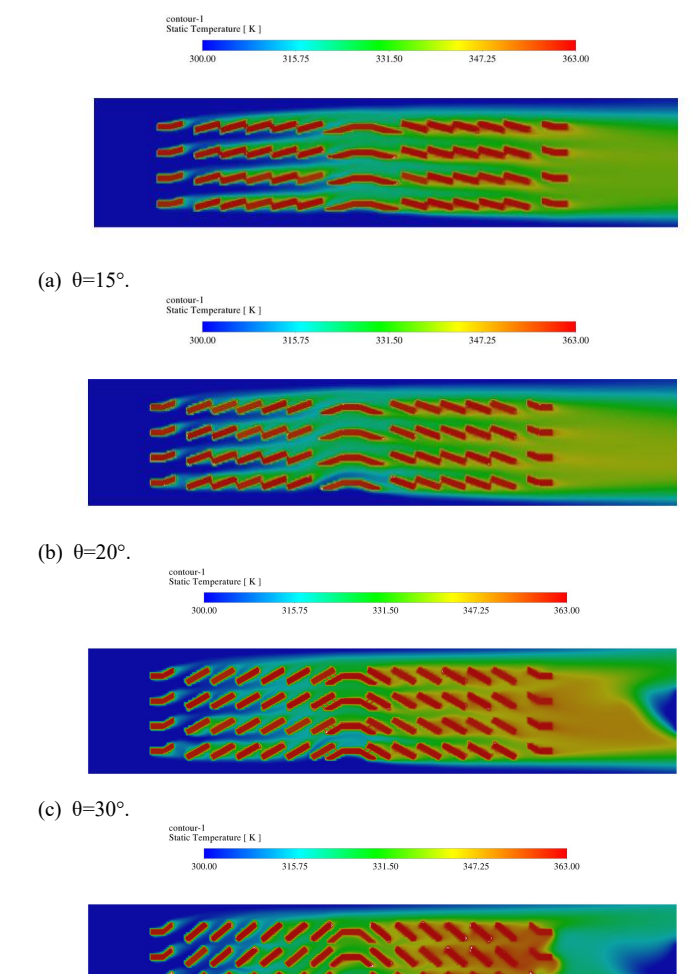


Fig. 10. Effect of louver opening angle on Ptotal at different wind speeds.

#### IV. HEAT TRANSFER RESULT ANALYSIS

#### A. Temperature Field and Velocity Field Analysis

Fluent was used to simulate heat transfer in the radiator, generating temperature contours of the fins' cross-section. Figure 11 shows the temperature distribution across the radiator cross-section at an incoming flow velocity of 14 m/s.



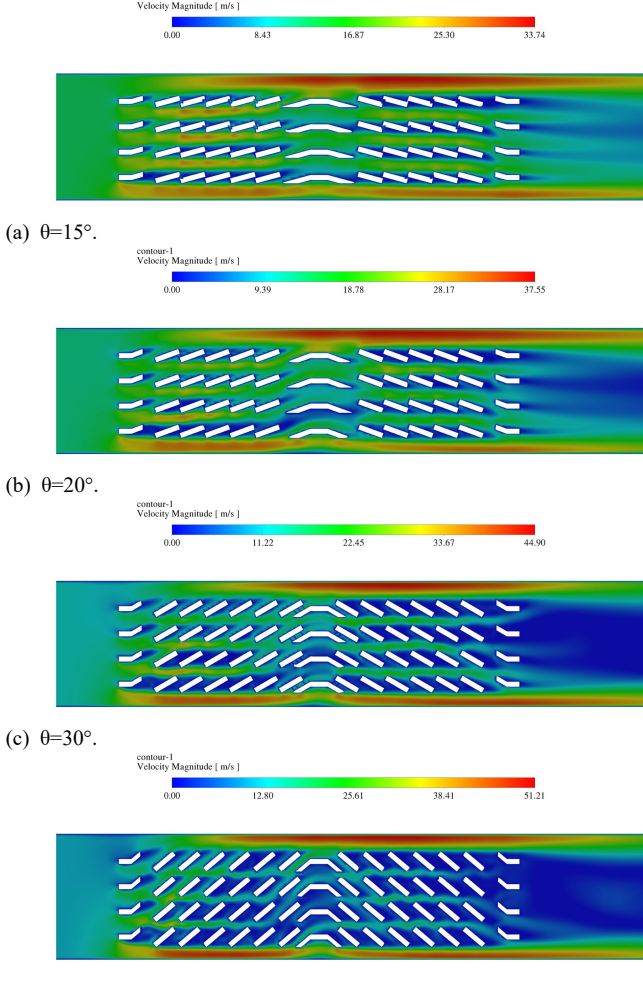
(d) θ=40°

Fig. 11. Cross-sectional temperature contours for different louver angles at a wind speed of 14 m/s.

The figure shows that as the louver angle increases, the heat transferred to the incoming airflow rises. This is reflected in the temperature contour by a gradual reduction in

the low-temperature region near the inlet (left side) and an expansion of the high-temperature region near the outlet (right side). This trend indicates that larger louver angles improve heat transfer performance. However, beyond a louver angle of 20°, the outlet temperature stabilizes, suggesting that further increases in the angle significantly elevate airflow resistance. This impedes airflow through the louvered structure, limiting further enhancements in heat transfer performance.

Figure 12 displays the velocity field across the radiator cross-section at an incoming flow velocity of 14 m/s. As the louver angle increases, the average flow velocity in the flow domain around the fins rises, while the main channel velocity decreases. At a louver angle of 30°, airflow accumulates near the upper and lower boundaries of the radiator, significantly reducing the outlet main channel velocity. This suggests that while larger louver angles enhance local airflow velocity, excessive angles cause uneven airflow and complex flow paths, destabilizing the main channel flow. These findings align with the temperature field variations in Figure 11, highlighting the role of fluid resistance and velocity changes in heat transfer performance.



(d) θ=40°

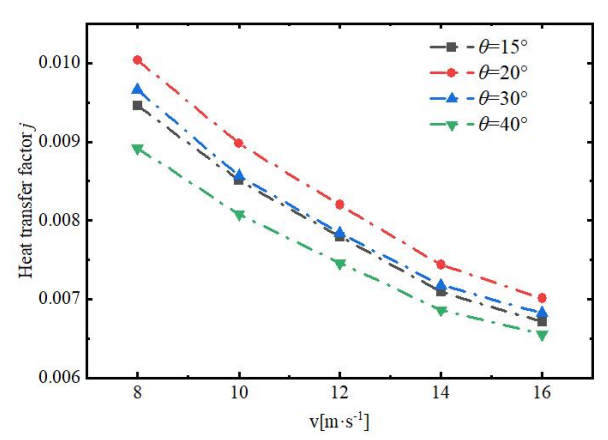
Fig. 12. Cross-sectional temperature contours for different louver angles at a wind speed of 14 m/s.

#### B. Heat Transfer Evaluation Factor Analysis

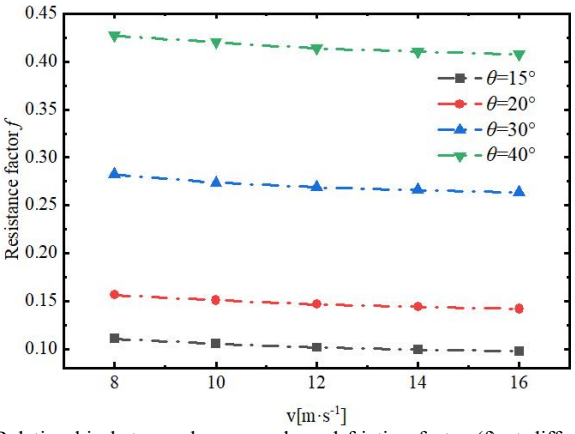
Figures 13 and 14 show the effects of louver angle on the Colburn j-factor (heat transfer performance) and friction factor (flow resistance) across various incoming flow

velocities. For a fixed louver angle, both the j-factor and friction factor decrease as flow velocity increases, likely due to enhanced turbulence. Under high-speed conditions (e.g., 16 m/s compared to 8 m/s), the j-factor for the 15° louver decreases by 29% and the friction factor by 12%, while for the 40° louver, they decrease by 26.5% and 4.5%, respectively.

At a constant flow velocity of 14 m/s, the j-factor initially increases with louver angle, peaking at 20° (8.3% higher than the value at 40°), before declining. Meanwhile, the friction factor rises sharply with larger angles, with the 40° louver exhibiting a value 341% higher than the 15° louver. This highlights the significant influence of louver angle on flow resistance. Thus, in radiator design, a moderate louver angle is recommended to optimize heat transfer performance while minimizing pressure drops and energy losses.



(a) Relationship between louver angle and heat transfer factor (j) at different incoming flow velocities.



(b) Relationship between louver angle and friction factor (f) at different incoming flow velocities.

Fig. 13. Effects of louver angle on j and f under different wind speeds.

To evaluate the combined effects of louver angle on heat transfer and flow resistance, the JF factor (a dimensionless index integrating j-factor and friction factor) is introduced. Figure 14 illustrates how louver angle affects the overall performance of the fins across various flow velocities. As flow velocity increases, the JF factor decreases across all louver angles, indicating that under high-load conditions, the balance between heat transfer and resistance becomes less favorable. At a fixed velocity, the JF factor declines as the louver angle rises from 15° to 40°, with the 15° louver outperforming the 40° louver by 66.4%, underscoring the advantage of smaller angles for overall performance.

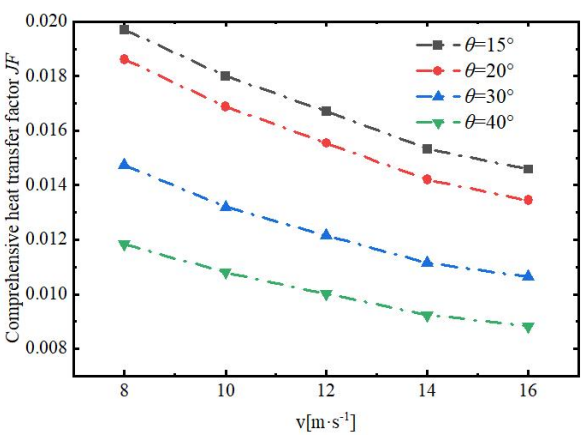


Fig. 14. Effects of louver angle on JF under different incoming flow

# V. COMPREHENSIVE ACOUSTIC THERMAL PERFORMANCE INDEX BASED ON THE ENTROPY WEIGHT METHOD

# A. Determination of the Comprehensive Acoustic Thermal Performance Index

In the design of louvered radiators, it is essential to maintain optimal heat transfer performance while minimizing noise levels. To quantify and intuitively analyze the balance between these two objectives, this study proposes a comprehensive performance index, Pm. This index is designed to quantify the combined effects of acoustic and thermal performance, providing a scientific basis for further optimization.

As a widely utilized objective weighting method, the core principle of the entropy weight method is to assign weights based on the degree of dispersion in each index's data. This method posits that if the variation in data for a particular indicator is significant — indicating greater dispersion — a higher weight should be assigned in the comprehensive evaluation. Conversely, if the variation in data for an indicator is minimal—indicating greater concentration—the weight should be correspondingly reduced. In this chapter, the entropy weight method is employed to determine the respective weights of the noise index and the heat transfer index within the comprehensive performance index.

Firstly, the noise evaluation index (Pa) and the comprehensive heat transfer factor (JF) are standardized. A higher noise evaluation index (Pa) indicates poorer noise performance, while a higher comprehensive heat transfer factor (JF) signifies better heat transfer performance. Consequently, it is necessary to process the positive and negative indicators. To achieve this, the range change method is employed to conduct a linear analysis of both the noise evaluation index (Pa) and the comprehensive heat transfer factor (JF). This method provides a more accurate representation of how structural parameters influence the comprehensive acoustic-thermal performance of the radiator. Within this analytical framework, when the index is maximized, Formula 12 is utilized:

$$y_{ij} = \frac{x_{ij} - \min(x_{ij})}{\max(x_{ij}) - \min(x_{ij})} + 0.001$$
 (12)

When the index is minimized, Formula 13 is utilized.

$$y_{ij} = \frac{\max(x_{ij}) - x_{ij}}{\max(x_{ij}) - \min(x_{ij})} + 0.001$$
 (13)

In the formula,  $x_{ij}$  and  $y_{ij}$  represent the simulation value and the standard value of the i-th sample under the j-th index, respectively. The terms  $\max(x_{ii})$  and  $\min(x_{ii})$  denote the maximum and minimum values of  $x_{ij}$ , respectively. To prevent the occurrence of zero values that could result in an inability to find a solution for the subsequent weight distribution, the normalized results are uniformly increased by more than two orders of magnitude for non-negative processing.

For the standardized data, the next step is to calculate the proportion of each sample value for each indicator. The proportion of the i-th sample under the j-th index is denoted as  $p_{ii}$ , which is calculated by dividing the sample value by the sum of all sample values under that index. The calculation formula is presented in Equation 14.

$$p_{ij} = \frac{y_{ij}}{\sum_{i=1}^{n} y_{ij}} \tag{14}$$

In the formula, n represents the number of samples. After calculating the proportion of each sample value for each index, the information entropy of each index can be determined. The information entropy is denoted as  $E_i$ . For the j-th index, the formula for calculating information entropy is as follows:

$$E_{j} = -k \sum_{i=1}^{n} (p_{ij} \ln(p_{ij}))$$

$$k = \frac{1}{\ln(n)}$$
(15)

$$k = \frac{1}{\ln(n)} \tag{16}$$

Where k is a constant used to normalize the entropy to a specific interval. A larger value of information entropy indicates greater dispersion of the data associated with the index, which in turn signifies a higher amount of information provided. Consequently, the weight assigned should also be increased.

The information entropy redundancy  $D_i$  for each index is calculated. A higher value of information entropy redundancy indicates a greater degree of data variation for the index, which enhances its significance in the comprehensive evaluation. Consequently, its weight should also be increased, as demonstrated in Equation 17.

$$D_{\cdot \cdot} = 1 - E_{\cdot \cdot} \tag{17}$$

The weight of each index is calculated based on information entropy redundancy. The weight  $w_i$  of each index is equal to its information entropy redundancy divided by the sum of the information entropy redundancy of all indices. This can be expressed as follows:

$$w_j = \frac{D_j}{\sum_{i=1}^n D_j} \tag{18}$$

In this chapter, there are only two indices: the noise evaluation index and the comprehensive heat transfer factor. After calculations using the entropy weight method, the weights are determined to be 0.56 and 0.44, that is:

$$P_{\rm m} = 0.56P_{\rm a} + 0.44JF \tag{19}$$

# B. The Relationship Between the Comprehensive Performance Index and Louver Opening Angle

Figure 15 illustrates the relationship between the comprehensive acoustic thermal performance of the radiator and the opening angle of the louver at various inflow velocities. The analysis indicates that the comprehensive acoustic thermal performance of the radiator exhibits a significant decline when transitioning from low-speed to high-speed conditions. Under high-speed conditions, the comprehensive performance of the radiator decreases by 49.9% to 60.3%. This trend demonstrates that higher flow velocities adversely affect the acoustic thermal performance of the radiator.

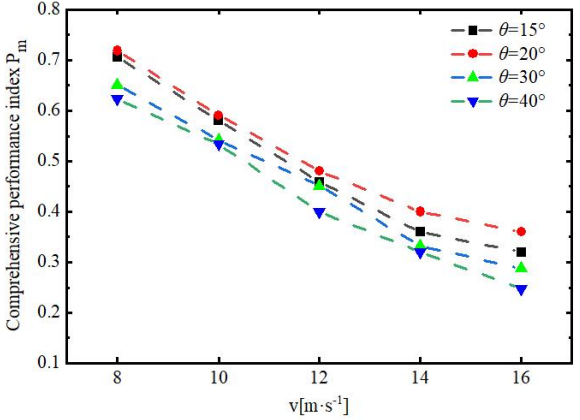


Fig. 15. Effect of louver window angle on overall performance index at different flow velocities

Focusing on the same working conditions with an incoming flow velocity of 14 m/s, the radiator with a window angle of 20° demonstrates the highest overall performance, which is 25% greater than that of a 40° angle. This improvement is attributed to the radiator's ability to enhance heat dissipation while maintaining low noise levels. In contrast, increasing the shutter opening angle to 40° reduces noise but significantly diminishes the effectiveness of heat dissipation. Therefore, to optimize both acoustic and thermal performance, it is recommended to utilize a shutter opening angle of 20° to achieve the best balance between noise reduction and heat dissipation efficiency.

# VI. CONCLUSIONS

This study utilized numerical simulations to investigate the effects of four commonly used louver angles on the heat transfer characteristics and noise performance of radiators. The primary conclusions are as follows:

- 1) Noise Performance: The noise performance of the radiator under high load conditions is generally inferior to that under low load conditions. Under identical circumstances, the comprehensive noise index  $P_a$  decreases as the window angle increases. Specifically, the comprehensive noise index  $P_a$  for the  $15\,^\circ$  louver is 42.45% higher than that for the  $40\,^\circ$  louver, indicating that a larger window angle contributes to improved noise performance of the radiator.
- 2) Heat Transfer Performance: The comprehensive heat transfer factor (JF) of the radiator under high-load conditions is generally lower than that under low-load conditions. Under identical conditions, JF decreases as the louver angle increases. Notably, the JF evaluation index for the 15° louver

is 66.4% higher than that for the 40° louver, suggesting that smaller louver angles are advantageous for enhancing heat transfer performance.

3) Comprehensive Performance Evaluation: The results of the entropy weight method indicate that the comprehensive performance of the radiator with a window angle of  $20^{\circ}$  is the highest, surpassing that of the radiator with a window angle of  $40^{\circ}$  by 25%. This angle achieves an optimal balance between noise level and heat dissipation efficiency.

In this study, we examine factors such as the common angles and time costs associated with the louvered windows of radiators in engineering vehicles. Four groups of commonly used radiator window angles are selected for research, providing a scientific basis for the structural optimization design of engineering vehicle radiators. It is recommended that a louver window angle of approximately 20 ° be preferred in practical applications to achieve an optimal balance between noise reduction and heat dissipation efficiency.

#### REFERENCES

- Zeng Zhixin, Feng Bo, Cui Zhenhua, et al. "Study on aerodynamic noise of radiator fan and improvement of bionics," Mechanical Science and Technology for Aerospace Engineering, 2022, 41(06): 954-960.
- [2] Zarri A, Christophe J, Moreau S, et al. "Influence of swept blades on low-order acoustic prediction for axial fans," Acoustics. MDPI, 2020, 2(4): 812-832.
- [3] Rydlewicz W, Rydlewicz M, Pałczyński T. "Experimental investigation of the influence of an orifice plate on the pressure pulsation amplitude in the pulsating flow in a straight pipe," Mechanical Systems and Signal Processing, 2019, 117: 634-652.
- [4] Xie Hui, Ge Xiyun, Liu Jian, et al. "Throttling and Acoustic Characteristics of Throttling Orificeplate with Different Configurations," Journal of Xi'an Jiaotong University, 2018, 52(06): 55-61.
- [5] Bi J, Liu J, Jiang Y. "Signal-to-noise research on comprehensive performance of plate heat exchanger for commercial electric vehicle," International Journal of Thermal Sciences, 2021, 165: 106967.
- [6] Zarri A, Botana M B, Christophe J, et al. "Aerodynamic investigation of the turbulent flow past a louvered-fin-and-tube automotive heat exchanger," Experimental Thermal and Fluid Science, 2024, 155: 111182.
- [7] Amoiridis O, Zarri A, Zamponi R, et al. "Sound localization and quantification analysis of an automotive engine cooling module," Journal of Sound and Vibration, 2022, 517: 116534.
- [8] Sanjosé M, Moreau S. "Fast and accurate analytical modeling of broadband noise for a low-speed fan," The Journal of the Acoustical Society of America, 2018, 143(5): 3103-3113.
- [9] Hu D, Dong W, Gao P, et al. Noise reduction optimization for numerous radiator fans for fuel cell vehicle considering thermal-fluid-acoustic synergy[J]. International Journal of Heat and Mass Transfer, 2024, 223: 125231.
- [10] Park M, Lee D J, Lee H. Experimental and computational investigation of the effect of blade sweep on acoustic characteristics of axial fan[J]. Applied Acoustics, 2022, 189: 108613.
- [11] Wang S, Yu X, Shen L, et al. Noise reduction of automobile cooling fan based on bio-inspired design[J]. Proceedings of the Institution of Mechanical Engineers, Part D: Journal of Automobile Engineering, 2021, 235(2-3): 465-478.
- [12] Zhang Ruijia, Zhang Yaping, Yin Renpan, et al. "Numerical Optimization of Flow and Heat Transfer Characteristics of Pin-Fin Radiator Module," Science Technology and Engineering, 2024, 24(05): 1923-1929.
- [13] Cao Kan, Yuan Yaohua, Wang Chunyan, et al. "Numerical simulation of staggered finned heat exchanger with perforated louvers," Cryogenics & Superconductivity, 2021, 49(11): 41-46,51.
- [14] Xie Wenyuan, Lv Xiaochen, Li Long, et al. "Flow and Thermal Characteristics Research on Hierarchical Manifold Microchannel Heat Sink Array," Spacecraft Engineering, 2020, 29(04): 99-107.
  [15] Yu Wan, Han Yu, Wang Gang, et al. "Analysis of the heat dissipation
- [15] Yu Wan, Han Yu, Wang Gang, et al. "Analysis of the heat dissipation performance of U-shaped flat plate micro-heat pipe LED radiator,"

- Transactions of the Chinese Society of Agricultural Engineering (Transactions of the CSAE), 2024, 40(9): 227-2357.
- [16] Wang Di, Min Chunhua, Yang Xuguang, et al. "Research on natural convection heat dissipation performance of electronic component radiator fins," Journal of Thermal Science and Technology, 2021,20(04):313-317.
- [17] Chen Huilan, Chen Yuehao, Wang Zixuan, et al. "Numerical simulation of flow heat transfer in water-cooled radiators with perforated fins," Cryogenics & Superconductivity, 2024, 52(10): 91-98.
- [18] Zhu Maotao, Yao Peng, Tian Chunhu, et al. "Optimization Design of Radiator Louver Fin Performance," Machinery Design & Manufacture, 2020, (12): 184-186, 190.
- [19] Tang Jingchun, Jiang Ying, Ye Bing, et al. "An experimental study on air-side heat transfer and resistance characteristics for ribbon-tubular radiator," Journal of Hefei University of Technology(Natural Science), 2023, 46(03): 308-312.
- [20] Yoo B K, Kim M S, Bang Y I, et al. Numerical analysis and correlation of thermohydraulic characteristics of louvered fin-tube heat exchanger[J]. International Journal of Refrigeration, 2023, 147: 121-133.
- [21] Zhang X, Huang Y, Song J, et al. Numerical investigation of the air-side performance of louver fin-and-tube radiators having rectangular, tapered and airfoil section configuration[J]. Energy Reports, 2022, 8: 11799-11809.
- [22] Yu C, Zhang W, Shao M, et al. CFD modeling and optimal design of louvered fins heat exchangers using radical basis function[J]. Case Studies in Thermal Engineering, 2024, 60: 104832.
- [23] Wang Dong, Zhang Xueliang, Li Qi. "Numerical simulation on aerodynamic noise of Helmholtz resonator," Computer Aided Engineering, 2012,21(6):5-10.
- [24] Yun J Y, Lee K S. "Influence of design parameters on the heat transfer and flow friction characteristics of the heat exchanger with slit fins," International Journal of Heat and Mass Transfer, 2000, 43(14): 2529-2539.
- [25] Li Qian, Ji Hua, Feng Donglin, et al. "Effects of hole distribution on flow field and noise for multi-hole plates," The Chinese Journal of Process Engineering, 2022, 22(05): 601-611.
- [26] Zhu Penghui, Jiang Jinhui, Cui Wenxu. "Analysis of Rotor Vibration Response and Noise Based on Two-Way Fluid-Structure Coupling," Journal of Nanjing University of Aeronautics and Astronautics(Natural Science Edition), 2024,56(02):242-252.
- [27] Paruchuri C, Subramanian N, Joseph P, et al. "Broadband noise reduction through leading edge serrations on realistic aerofoils," 21st AIAA/CEAS Aeroacoustics Conference, 2015: 2202.
- [28] Asghar A, Perez R E, Jansen P W, et al. "Application of leading-edge tubercles to enhance propeller performance," AIAA Journal, 2020, 58(11): 4659-4671.

Jie Meng, male. The author is an Associate Professor at Taiyuan University of Science and Technology. Meng was born in China. In 2018, he received his PhD in Mechanical Engineering from Taiyuan University of Science and Technology, Shanxi Province, China. Mainly research topics: mechanical system dynamics analysis, mechanical structure design and optimization, and bionic mechanical research and application.

As an ASSOCIATE PROFESSOR, he is currently working at the School of Vehicle and Transportation Engineering, Taiyuan University of Science and Technology.

# Selected publications:

- (1) Jie Meng, Dagang Sun. "Research on Vibration Suppression of Wind Turbine Blade Based on Bamboo Wall Three-layer Damping Structure" Journal of Vibroengineering, 2017, vol. 19, pp. 87-99. (SCI)
- (2) Jie Meng, Dagang Sun. "Structural Optimization of Wind Turbine Blades with Ring Shear Webs" Journal of the Brazilian Society of Mechanical Sciences and Engineering, 2018, vol. 40, no. 313. (SCI)
- (3) Jie Meng, Yongxiang Mu, Xiaochang Ma. "Analysis on the Vibration Performance of Spruce Structure with Variable Cross-Section Under Snow Load by Semi-Analytical Method" International Journal of Structural Stabilityand Dynamics, 2023. (SCI)

#### His research interests:

Key technologies of large wind turbine blade dynamics and vibration suppression, vehicle chassis dynamics and structure optimization, bionic damping structure design, and vibration and noise reduction technology.